

Cross-Dataset Gaze Estimation by Evidential Inter-intra Fusion

Shijing Wang
Beijing Jiaotong University
Beijing, China
shijingwang@bjtu.edu.cn

Yaping Huang*
Beijing Jiaotong University
Beijing, China
yphuang@bjtu.edu.cn

Jun Xie
Lenovo
Beijing, China
xiejun@lenovo.com

Yi Tian
Beijing Jiaotong University
Beijing, China
tianyi@bjtu.edu.cn

Feng Chen
Lenovo
Beijing, China
chenfeng13@lenovo.com

Zhepeng Wang
Lenovo
Beijing, China
wangzpb@lenovo.com

ABSTRACT

Achieving accurate and reliable gaze predictions in complex and diverse environments remains challenging. Fortunately, it is straightforward to access diverse gaze datasets in real-world applications. We discover that training these datasets jointly can significantly improve the generalization of gaze estimation, which is overlooked in previous works. However, due to the inherent distribution shift across different datasets, simply mixing multiple dataset decreases the performance in the original domain despite gaining better generalization abilities. To address the problem of “cross-dataset gaze estimation”, we propose a novel **Evidential Inter-intra Fusion (EIF)** framework, for training a cross-dataset model that performs well across all source and unseen domains. Specifically, we build independent single-dataset branches for various datasets where the data space is partitioned into overlapping subspaces within each dataset for local regression, and further create a cross-dataset branch to integrate the generalizable features from single-dataset branches. Furthermore, evidential regressors based on the Normal and Inverse-Gamma (NIG) distribution are designed to additionally provide uncertainty estimation apart from predicting gaze. Building upon this foundation, our proposed framework achieves both intra-evidential fusion among multiple local regressors within each dataset and inter-evidential fusion among multiple branches by **Mixture of Normal Inverse-Gamma (MoNIG)** distribution. Experiments demonstrate that our method consistently achieves notable improvements in both source domains and unseen domains.

CCS CONCEPTS

• **Human-centered computing** → **User models.**

KEYWORDS

Gaze Estimation, Cross-Dataset Training, Evidential Fusion

1 INTRODUCTION

Gaze estimation is an important task in computer vision used to determine where a person is looking based on visual cues. It has gained attention for its wide range of applications in human-computer interaction [27, 29], virtual reality [20, 28], and assistive technology [11, 18, 23].

The challenge of gaze estimation primarily lies in the complexity and diversity of real-world environments. In fact, existing datasets [13, 19, 38, 39] are collected in different environments,

*Corresponding author.

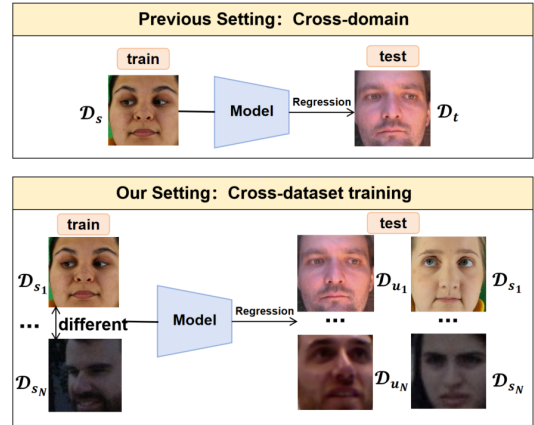


Figure 1: Comparison between traditional *Cross-Domain* scenario and our *Cross-Dataset Training* scenario. Here, \mathcal{D}_s represents the source domain, \mathcal{D}_t represents the target domain, and \mathcal{D}_u represents the unseen domain. *Cross-Dataset Training* involves training on multiple source domains with significant distribution discrepancies, aiming for consistent performance across these source domains and the unseen domains.

resulting in notable variations in data distribution among them. To enhance the model’s generalization ability across multiple scenarios, current research [3–5, 7, 16, 22, 24, 33] focuses on studying cross-domain scenarios and improving performance through single-source domain adaptation and domain generalization strategies, achieving promising progress. However, in practical applications, we often have easy access to multiple data sources, so it is natural to expect models trained on these datasets to perform well across all these source domains as well as unseen domains. This issue is known as cross-dataset training, and Fig. 1 illustrates the differences between our setting and traditional cross-domain setting. While cross-dataset training has been extensively studied in many fields such as object detection [6, 35, 35], semantic segmentation [30, 32], facial expression recognition [37] and trajectory prediction [15], it has received little attention in gaze estimation.

Preliminary experiments depicted in Fig. 2 show that simply combining data (e.g., Gaze360+ETH-Gaze, shorted as G+E) from multiple datasets can significantly enhance the model’s performance

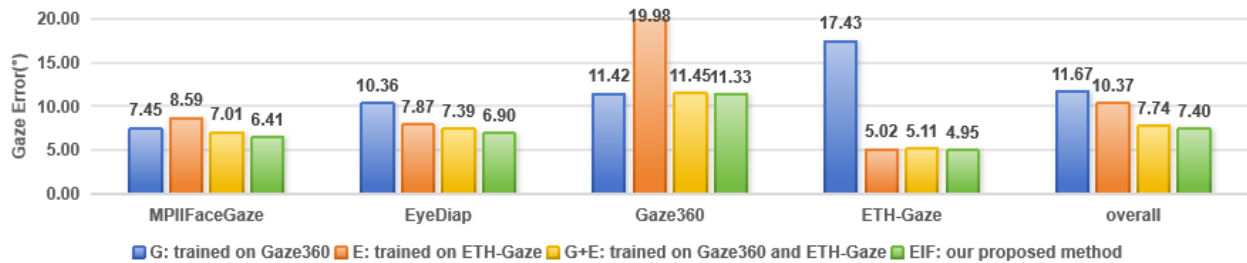


Figure 2: Test accuracy on different datasets with varied combination of training data.

on unseen domains (e.g., MPIIFaceGaze, EyeDiap), even outperforming carefully designed state-of-the-art (SOTA) single-source domain generalization methods [4, 7]. This improvement is due to the diverse data distributions across source domain datasets. By merging these datasets, we increase the variety of the training data, which largely enhances the model’s generalization ability to unseen domains. Unfortunately, despite increasing the volume of training data, cross-dataset training results in diminished performance on test sets of the original source domains (Gaze360, ETH-Gaze) compared to training exclusively with their own training data. This decrease is also attributed to the significant differences in data distribution among source domains, but need to be mitigated.

To prevent the degradation of source domain performance and further enhance performance on unseen domains, in this paper, we propose a novel solution called Evidential Inter-intra Fusion (EIF) for cross-dataset gaze estimation. Acknowledging the inherent differences between the datasets, our approach involves training independent single-dataset branches for each dataset, thereby mitigating source domain performance degradation. Additionally, building upon the findings from preliminary experiments, which suggest that merging rich source domain information benefits unseen domains, we devise a cross-dataset branch containing only the deep layers, where the generalizable features from each source domain branch are integrated, thereby boosting performance on unseen domains. On the other hand, to combat the performance drop in the source domains, we argue that the non-stationary gazing process inherent in each dataset should be carefully considered, where non-stationary refers to our gaze being primarily influenced by head posture and eye movement with their effects varying across different gaze ranges. Such challenge is tackled by proposing to partition the data space into overlapping subspaces, with an independent local regressor assigned to each subspace. Furthermore, in order to select appropriate regressors both in within-dataset and cross-dataset branches, we design to employ evidential regressors based on the Normal and Inverse-Gamma (NIG) distribution for not only predicting gaze but also offering uncertainty estimation. Leveraging the Mixture of Normal Inverse-Gamma (MoNIG) distribution, our framework achieves both intra-evidential fusion among numerous local regressors within each dataset and inter-evidential fusion across multiple-dataset branches.

During training, to enable the model to rapidly adapt to variations in the number of datasets, the training process of our proposed EIF is divided into two stages. In stage 1, we train each single-dataset

branch separately. In stage 2, we create a cross-dataset branch and jointly train all branches for only a few epochs. During inference, the predictions including both gaze and uncertainty are output, which largely enhance the reliability of our proposed framework. We thoroughly evaluate the effectiveness of our proposed EIF on established gaze estimation benchmarks.

In summary, our contribution is three-fold:

- We introduce the task of cross-dataset training for the first time in the field of gaze estimation, which can significantly improve the generalization of gaze estimation.
- We propose a novel framework, called Evidential Inter-intra Fusion (EIF), which consists of several single-dataset branches and a cross-dataset branch, to tackle the challenge in cross-dataset gaze estimation. EIF is equipped with multiple local regressors fused by intra-evidential within each dataset and meanwhile performs inter-evidential fusion across multiple datasets, ensuring accurate gaze estimation in complex and diverse environments.
- We conduct comprehensive experiments that demonstrate the consistent performance improvement in both source domains and unseen domains.

2 RELATED WORK

2.1 Gaze Estimation

Gaze estimation methods can be divided into two main types [17]: model-based and appearance-based approaches. Model-based methods [1, 31] rely on the accurate reconstruction of 3D model of the eyes, thus requiring specialized equipments such as depth sensors, infrared cameras, and lighting. By contrast, appearance-based methods [9] estimate gaze using images captured by a single webcam, and thus facilitate the popularity of gaze estimation. With advancements in deep learning, appearance-based methods have significantly improved the performance and garnered widespread attention. However, deep learning methods heavily rely on data that can ideally reflect the distribution of real-world conditions. Yet, the actual gaze estimation scenario is diverse and complex [14].

In fact, the current gaze datasets are collected in various environments, resulting in significant differences in data distribution. For example, MPIIFaceGaze [39] is collected during the natural use of the laptops, with images captured using the laptop camera. EyeDiap [13], on the other hand, is collected in laboratory settings,

where participants are instructed to observe given targets, and images are captured using depth cameras. Gaze360 [19] is collected in the wild using a 360-degree camera to simultaneously record multiple participants. Lastly, ETH-Gaze [38] is constructed in a laboratory green screen environment, where lighting conditions are simulated using controlled lighting, and images are captured using ultra-high-resolution cameras.

Due to variations in data distributions among datasets, traditional deep learning methods often struggle in cross-domain scenarios. Many researches focus on employing domain generalization and domain adaptation strategies to alleviate the effect of domain discrepancy. Liu *et al.* [24] propose outlier-guided collaborative adaptation. Wang *et al.* [33] introduce regression contrastive learning techniques. Bao *et al.* [3] propose a rotation consistency strategy. Cheng *et al.* [7] utilize adversarial reconstruction techniques to purify gaze features. Cai *et al.* [5] attempt to reducing sample and model uncertainty. Bao *et al.* [4] propose constructing Physics-Consistent Features (PCF) to incorporate physical definition.

Unlike the methods mentioned above, our work introduces a novel practical scenario called cross-dataset training. In this scenario, we have access to data from multiple source domains collected in different environments with distribution variations during training, which significantly improves cross-domain performance without sacrificing performance of within-domain.

2.2 Cross-dataset Training

In many computer vision tasks, researches on cross-dataset training have been well-explored, but they face different challenges compared to “cross-dataset gaze estimation”. For instance, in object detection, the main challenge lies in the disparate definitions and granularity of classes across different datasets. Therefore, the focus of related works [6, 30, 35] is on integrating diverse datasets into a unified taxonomy. In the field of facial expression recognition, a primary challenge in cross-dataset training stems from the inconsistent annotations among datasets. To address this issue, the method [37] learns a transition matrix for modeling the relationship between the latent ground truth and the dataset annotation.

Unlike the tasks mentioned above, the challenge need to be solved in cross-dataset gaze estimation is the inherent distribution shift across different datasets. Similar challenges have also been identified in semantic segmentation for autonomous driving by Wang *et al.* [32]. They propose a solution based on the characteristics of their task, which involves training independent batch normalization (BN) layers for each dataset while sharing their convolutional layers. However, it requires prior knowledge of which source domain the test sample belongs to for selecting the corresponding BN layer during testing. In contrast, our objective is to enable testing in both the source domains and unseen domains for gaze estimation task without requiring to know which corresponding source domain dataset a test sample belongs to.

3 METHODS

In this section, we elaborate the proposed Evidential Inter-intra Fusion (EIF) framework. As depicted in Fig. 3, EIF model incorporates multiple **single-dataset branches**, each dedicated to a

distinct source domain dataset. Additionally, to enhance performance on unseen domains, we introduce a **cross-dataset branch** that aggregates features from all source domain branches. To address the performance degradation of source domain caused by non-stationary nature of the gazing process, we draw inspiration from similar challenges addressed in other tasks such as age estimation [21], action quality assessment [36], equipping each branch with multiple **local regressors** tailored to specific data subspaces. Subsequently, we employ **intra-evidential fusion module** to fuse local regressors within each branch and **inter-evidential fusion module** to fuse multiple branches. In the following subsections, we will delve into the components of the framework, encompassing the single-dataset branch, cross-dataset branch, evidential fusion module, and the two-stage training process.

3.1 Single-dataset Branch

Due to the inherent distributional shifts among datasets, each single-dataset branch is tailored to a specific source domain dataset. It includes several layers for feature extraction and two regression layers, R_1 and R_2 , designed to estimate the two components of gaze: yaw (Y_1) and pitch (Y_2). Since these layers have the same structure, differing only in the gaze components they estimate, we will use R for the regression layers and Y for the gaze components to introduce the model structure conveniently in the following description.

Recognizing the non-stationary nature of gaze behavior might lead to the performance drop when combining multiple datasets, we design the regression layer R to include multiple local regressors, denoted as $R = \{r_1, r_2, \dots, r_G\}$. These local regressors operate exclusively within specific data subspaces, which are partitioned based on gaze labels Y , and thus can be viewed as a collective of experts, with each expert specializing in specific regression scenarios.

Moving forward, the method of obtaining data subspaces by gaze label R is crucial. Since gaze labels are not uniformly distributed, simply dividing the entire range equitably may result in an imbalanced data distribution among the subspaces. To tackle this issue, we introduce a density-based partitioning approach. Initially, we sort the gaze labels $Y = \{y^1, y^2, \dots, y^S\}$ in ascending order to achieve $Y^* = \{y^{1^*}, y^{2^*}, \dots, y^{S^*}\}$. Subsequently, we sample indices at regular intervals to identify the centers of each gaze group:

$$\zeta_{\text{center}}^g = Y^* \left(\left\lfloor S \times \frac{(g + 0.5)}{G} \right\rfloor \right) \quad (1)$$

where ζ_{center}^g represents the center of the g -th gaze group, $Y^*(s)$ indicates the s -th element in Y^* , with indexing starting from 1, S is the total count of samples, g is the index of the gaze group, and G signifies the total number of gaze groups. The $\lfloor \cdot \rfloor$ function signifies the floor operation, ensuring indices are integers.

Additionally, we employ a dense overlap strategy among gaze groups, enabling adjacent groups to have overlapping intervals. This strategy ensures that data within overlapping regions contribute to training multiple regressors, thereby enhancing model robustness and accuracy across varying gaze behaviors. The degree of overlap between them is determined by a dense overlap coefficient denoted by α . Formally, the boundaries for each group are

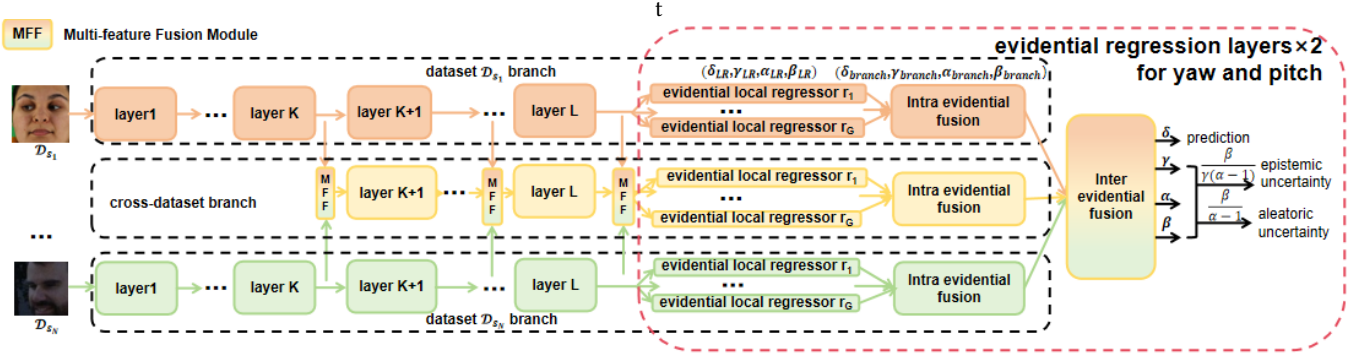


Figure 3: Illustration of the proposed Evidential Inter-intra Fusion (EIF) framework. The model consists of multiple single-dataset branches and a cross-dataset branch, with each branch comprising multiple local regressors. We utilize the intra-evidential fusion module to perform local regressor fusion within each branch and the inter-evidential fusion module to perform fusion across multiple branches. The output includes both predictions and uncertainty. Due to gaze estimation involving yaw and pitch components, there are two identical regression layers with the same model structure.

defined as follows:

$$\begin{aligned} \zeta_{\text{left}}^g &= Y^* \left(S \times \frac{(g + 0.5 - 0.5 \times \alpha)}{G} \right), \\ \zeta_{\text{right}}^g &= Y^* \left(S \times \frac{(g + 0.5 + 0.5 \times \alpha)}{G} \right), \\ \mathcal{I}^g &= (\zeta_{\text{left}}^g, \zeta_{\text{right}}^g). \end{aligned} \quad (2)$$

Here, \mathcal{I}^g is boundaries of the g -th gaze group. We set $\alpha > 1$ to ensure that each gaze group has an overlap interval. By partitioning the gaze groups in this manner, data with gaze label y_s that fall within $(\zeta_{\text{left}}^g, \zeta_{\text{right}}^g)$ are utilized for training the branch r_g , and the output range of r_g is also constrained to $(\zeta_{\text{left}}^g, \zeta_{\text{right}}^g)$.

3.2 Cross-dataset Branch

To improve performance in unseen domains, preliminary experiments have demonstrated that utilizing data from various source domains can significantly boost the model’s effectiveness in such scenarios. This insight leads to the creation of the cross-dataset branch, a key component designed to combine information from different data sources. The cross-dataset branch is equipped with multiple Multi-Feature Fusion (MFF) modules and regression layers, whose architecture mostly mirrors the higher layers of the single-dataset branch. The intuition behind this design is that the lower layers usually capture generalizable features across different datasets and higher layers capture dataset-specific features, so we preserve the features from lower layers, and only fuse the features from high layers for tuning the cross-dataset branch.

Formally, let f_n^l denote the l -th layer feature of the n -th source dataset branch. Assuming fusion of features from multiple source datasets begins at the K -th layer, the fusion process of the MFF module can be represented as:

$$f_{\text{cross}}^K = \text{MFF}_k(f_1^K, f_2^K, \dots, f_{S_N}^K), \quad (3)$$

where S_N is the total number of source datasets, and f_{cross}^K indicates the features output from K -th MFF layer.

After that, in the following MFF modules, we fuse features from all source dataset branches as well as the features output from the previous MFF module. This fusion process can be described as:

$$f_{\text{cross}}^{k+1} = \text{MFF}_k(f_1^k, f_2^k, \dots, f_{S_N}^k, f_{\text{cross}}^k), \quad (4)$$

where k ranges from K to $L - 1$, and L denotes the total number of layers for feature extraction in the single-dataset branch.

The inputs of MFF module come from different branches at the same layer, so their features are spatially aligned. But they may not be aligned in channels, hence, we first independently apply multiple point-wise convolutions to align features in channels. Subsequently, we use the Attention Feature Fusion (AFF) module proposed by Dai *et al.* [10] to fuse features pairwise (refer to [10] for details). The computation of k -th MFF module is expressed as:

$$\text{MFF}_k = \text{AFF}(\dots, \text{AFF}(\text{conv}(\cdot), \text{conv}(\cdot)), \dots, \text{conv}(\cdot)). \quad (5)$$

3.3 Evidential Fusion Module

In this section, we introduce both an intra-evidential fusion module for fusing multiple local regressors within each dataset and an inter-evidential fusion module for fusing multiple dataset branches. The evidential fusion module is based on evidence regression learning [2]. From its perspective, the gaze component y is sampled from a normal distribution, with the mean and variance sampled from normal and Inverse-Gamma (NIG) distributions, respectively. Therefore, y can be seen as indirectly sampled from an NIG distribution with parameters $\tau = (\delta, \gamma, \alpha, \beta)$, where $\delta \in \mathbb{R}$, $\gamma > 0$, $\alpha > 1$, and $\beta > 0$. This can be expressed as:

$$y \sim \mathcal{N}(\mu, \sigma^2), \quad \mu \sim \mathcal{N}(\delta, \sigma^2 \gamma^{-1}), \quad \sigma^2 \sim \Gamma^{-1}(\alpha, \beta), \quad (6)$$

where $\Gamma(\cdot)$ is a gamma function. All of our local regressors adopt the evidential approach which is implemented by a fully connected layer that outputs four numbers corresponding to δ , γ , α , and β . During training, the evidence learning loss $\mathcal{L}_{\text{evidence}}$ consists of two essential components: the negative log-likelihood \mathcal{L}_{NLL} and a regularization term \mathcal{L}_{R} . The negative log-likelihood \mathcal{L}_{NLL} is defined

as:

$$\begin{aligned} \mathcal{L}_{\text{NLL}}(\delta, \gamma, \alpha, \beta) &= \frac{1}{2} \log\left(\frac{\pi}{\gamma}\right) - \alpha \log(\Omega) \\ &+ \left(\alpha + \frac{1}{2}\right) \log\left((y - \delta)^2 \gamma + \Omega\right) \\ &+ \log\left(\frac{\Gamma(\alpha)}{\Gamma\left(\alpha + \frac{1}{2}\right)}\right), \end{aligned} \quad (7)$$

where $\Omega = 2\beta(1 + \gamma)$. The regularization term \mathcal{L}_{R} is introduced to penalize incorrect evidence predictions and is given by:

$$\mathcal{L}_{\text{R}}(\delta, \gamma, \alpha, \beta) = |y - \delta| \cdot (2\gamma + \alpha). \quad (8)$$

The total loss, denoted as $\mathcal{L}_{\text{total}}$, is obtained by combining the negative log-likelihood and regularization term:

$$\mathcal{L}_{\text{evidence}}(\delta, \gamma, \alpha, \beta) = \mathcal{L}_{\text{NLL}}(\delta, \gamma, \alpha, \beta) + \lambda \mathcal{L}_{\text{R}}(\delta, \gamma, \alpha, \beta), \quad (9)$$

where the coefficient $\lambda > 0$ balances the contributions of the two loss terms.

Building upon evidence regression learning, the evidential fusion module employs the Mixture of normal-inverse gamma distribution (MoNIG) [26] for fusion. The resulting distribution remains NIG, represented as:

$$\begin{aligned} \text{MoNIG}(\delta, \gamma, \alpha, \beta) &= \text{NIG}(\delta_1, \gamma_1, \alpha_1, \beta_1) \oplus \\ &\text{NIG}(\delta_2, \gamma_2, \alpha_2, \beta_2) \oplus \\ &\dots \oplus \text{NIG}(\delta_M, \gamma_M, \alpha_M, \beta_M), \end{aligned} \quad (10)$$

where M is the number of NIG distributions being fused, and the parameters are computed as:

$$\begin{aligned} \delta &= \frac{\sum_{i=1}^M \gamma_i \delta_i}{\sum_{i=1}^M \gamma_i}, \quad \gamma = \sum_{i=1}^M \gamma_i, \\ \alpha &= \sum_{i=1}^M \alpha_i + \frac{1}{M}, \quad \beta = \sum_{i=1}^M \beta_i + \frac{1}{M} \sum_{i=1}^M \gamma_i (\delta_i - \delta)^2. \end{aligned} \quad (11)$$

Given the outputs of the g local regressors in the n -th branch as $\text{NIG}_{\text{LR}_g}^n(\delta_{\text{LR}_g}^n, \gamma_{\text{LR}_g}^n, \alpha_{\text{LR}_g}^n, \beta_{\text{LR}_g}^n)$, the output of the n -th branch after the intra-evidential fusion module, NIG_{BR}^n , can be represented as:

$$\begin{aligned} \text{NIG}_{\text{BR}}^n(\delta_{\text{BR}}^n, \gamma_{\text{BR}}^n, \alpha_{\text{BR}}^n, \beta_{\text{BR}}^n) &= \text{NIG}_{\text{LR}_1}^n \oplus \\ &\text{NIG}_{\text{LR}_2}^n \oplus \dots \oplus \text{NIG}_{\text{LR}_G}^n. \end{aligned} \quad (12)$$

Similarly, the output of each branch are further fused by the inter-evidential fusion module, and the final output, $\text{NIG}(\delta, \gamma, \alpha, \beta)$, can be represented as:

$$\begin{aligned} \text{NIG}(\delta, \gamma, \alpha, \beta) &= \text{NIG}_{\text{BR}}^1 \oplus \dots \\ &\oplus \text{NIG}_{\text{BR}}^{\text{SN}} \oplus \text{NIG}_{\text{BR}}^{\text{cross}}, \end{aligned} \quad (13)$$

where $\text{NIG}_{\text{BR}}^{\text{cross}}$ corresponds to the output of the cross-dataset branch. Then, we can compute the prediction gaze, aleatoric, and epistemic uncertainties based on $\text{NIG}(\delta, \gamma, \alpha, \beta)$ as follows:

$$\underbrace{\mathbb{E}[\mu]}_{\text{gaze}} = \delta, \quad \underbrace{\mathbb{E}[\sigma^2]}_{\text{aleatoric}} = \frac{\beta}{\alpha - 1}, \quad \underbrace{\text{Var}[\mu]}_{\text{epistemic}} = \frac{\beta}{\gamma(\alpha - 1)}. \quad (14)$$

3.4 Two-stage Training Process

To enable the model to rapidly adapt to variations in the number of datasets, we devise a two-stage training strategy. In stage 1, we train each source domain branch separately. For each dataset branch, the corresponding source domain data is divided into G gaze groups \mathcal{I}^g based on Equation 2. The output of G local regressors for the s -th sample of the source domain data is denoted as $\delta_{\text{LR}_g}^s, \gamma_{\text{LR}_g}^s, \alpha_{\text{LR}_g}^s, \beta_{\text{LR}_g}^s$. We only compute $\mathcal{L}_{\text{local}}^g$ within the g -th gaze group data subspace corresponding to the g -th local regressor, as follows:

$$\mathcal{L}_{\text{local}}^g = \sum_{y^s \in \mathcal{I}^g} \mathcal{L}_{\text{evidence}}(\delta_{\text{LR}_g}^s, \gamma_{\text{LR}_g}^s, \alpha_{\text{LR}_g}^s, \beta_{\text{LR}_g}^s, y^s). \quad (15)$$

Here, y^s represents the gaze label of the s -th sample. Then, we compute the output of this dataset branch after intra-evidential fusion according to Equation 12, denoted as $\delta_{\text{BR}}^s, \gamma_{\text{BR}}^s, \alpha_{\text{BR}}^s, \beta_{\text{BR}}^s$. We compute the loss $\mathcal{L}_{\text{global}}$ for it across the entire source domain dataset as follows:

$$\mathcal{L}_{\text{global}} = \sum \mathcal{L}_{\text{evidence}}(\delta_{\text{BR}}^s, \gamma_{\text{BR}}^s, \alpha_{\text{BR}}^s, \beta_{\text{BR}}^s, y^s) \quad (16)$$

Therefore, during the first stage of training, the loss $\mathcal{L}_{\text{branch}}$ for each single-dataset branch is as follows:

$$\mathcal{L}_{\text{branch}} = \sum_{g=1}^G \mathcal{L}_{\text{local}}^g + \mathcal{L}_{\text{global}}. \quad (17)$$

In stage 2, we create a cross-dataset branch and jointly train all branches for only a few epochs. Specifically, we first merge multiple source domain datasets and then use Equation 2 to obtain G gaze groups $\mathcal{I}_{\text{cross}}^g$ for the cross-dataset branch. Then, we compute the loss $\mathcal{L}_{\text{cross}}$ for the cross-dataset branch according to Equation 17. Given the outputs of each single branch, we fuse them using Equation 13 to obtain $\delta^s, \gamma^s, \alpha^s, \beta^s$, and then compute the loss $\mathcal{L}_{\text{joint}}$ across all source domain datasets as follows:

$$\mathcal{L}_{\text{joint}} = \sum_{\mathcal{D}_{S_1} \dots \mathcal{D}_{S_N}} \mathcal{L}_{\text{evidence}}(\delta^s, \gamma^s, \alpha^s, \beta^s, y^s), \quad (18)$$

Therefore, the total loss for stage 2 is

$$\mathcal{L}_{\text{stage2}} = \mathcal{L}_{\text{cross}} + \mathcal{L}_{\text{joint}}. \quad (19)$$

4 EXPERIMENT

4.1 Cross-dataset Setting

The experiments utilize four widely used gaze estimation datasets, EyeDiap [13], MPIIFaceGaze [39], Gaze360 [19], and ETH-XGaze [38]. We pre-process the data following the technique in [9]. To facilitate comparisons, we reference the setup of cross-domain scenarios [5, 34] in our cross-dataset setting, *i.e.*, we choose ETH-XGaze and Gaze360, known for their wider gaze distributions, as the source domains, and MPIIGaze and EyeDiap as the unseen datasets. Specific details regarding the datasets are provided below.

ETH-Gaze (Source Domain): This dataset is captured in a laboratory environment using high-resolution cameras, comprising 756k training images from 80 subjects. Since the ETH-Gaze dataset lacks gaze target annotations for the test set, we redefine the dataset splits following the setup in [9]. Specifically, we split the original training set into two subsets and use them as training and testing sets, as done in previous works [8].

Table 1: Comparison of gaze estimation performance in terms of angle error (°) in domain generalization setting. The best, second best and third best results are denoted as red, blue and green respectively.

Method \ Test	Source Domain		Unseen Domain		Average	
	Gaze360	ETH-Gaze	MPIIFaceGaze	EyeDiap	Unseen	All
Baseline (ETH-Gaze)	19.98	5.02	8.59	7.87	8.23	10.37
Baseline (Gaze360)	11.42	17.43	7.45	10.36	8.91	11.67
Baseline (ETH-Gaze+Gaze360)	11.45	5.11	7.01	7.39	7.20	7.74
PureGaze (ETH-Gaze)	-	-	7.08	7.48	7.28	-
PureGaze (Gaze360)	-	-	9.28	9.32	9.30	-
GCF (ETH-Gaze)	-	-	6.50	7.44	6.97	-
GCF (Gaze360)	-	-	7.55	9.03	8.29	-
EIF (ETH-Gaze+Gaze360)	11.03	4.75	6.40	6.77	6.58	7.24

Gaze360 (Source Domain): This dataset is collected in both indoor and outdoor environments using a 360-degree camera. The dataset contains 84k training images from 54 subjects and 16k testing images from 15 subjects.

MPIIFaceGaze (Unseen Domain): This dataset is collected during natural laptop use, with images captured using the laptop camera. It comprises 45k images from 15 users.

EyeDiap (Unseen Domain): This dataset is collected in a laboratory environment, where participants are asked to gaze at two types of visual target sessions: screen target and 3D floating ball. It comprises a total of 16k images gathered from 16 users.

4.2 Implementation Details

We use ResNet-18 backbone following previous studies [4, 5, 7, 34]. All images are resized to 224×224 . The batch size is 128, and we use the Adam optimizer with a learning rate of 10^{-4} . In stage 1, we train on each source domain dataset for 100k batches. In stage 2, we perform joint training for only 5k batches using all source domain datasets. Considering the discrepancy in the quantity of data among source domain datasets, during the joint training in stage 2, instead of directly mixing multiple datasets for sampling, we adopt a balanced mixing approach, where the datasets with fewer samples are oversampling to balance the data across all source domain datasets. By default, we set the number of local regressors G to 8, the overlap coefficient α to 2.0, the evidence learning regularization loss λ to 0.01, and the starting MFF layer K in the cross-dataset branch to 3.

4.3 Domain Generalization Results

We trained our method on the source domains (ETH-Gaze and Gaze360 datasets) and compared it with three categories of methods:

Single-dataset baseline (ETH-Gaze, Gaze360): Networks trained using only a single source domain utilize the common L1 loss function for gaze estimation, while all other settings, including the network backbone and training parameters, remain consistent with our proposed method.

Cross-dataset baseline (ETH-Gaze+Gaze360): Network is trained by simply mixing the ETH-Gaze and Gaze360 datasets, and the network settings are the same as the single-dataset baseline.

Cross-domain methods (PureGaze, GCF): The state-of-the-art (SOTA) gaze estimation domain generalization methods include PureGaze [7] and GCF [34]. They are trained on a single source domain (ETH-Gaze or Gaze360) using carefully designed algorithms for domain generalization.

From Table 1, it can be observed that the cross-dataset training baseline (ETH-Gaze+Gaze360) achieves comparable performance with the carefully designed SOTA single-domain generalization methods on the unseen dataset. However, there is a slight error increase in the source domains. Fortunately, our proposed method EIF reduces gaze errors in both the source domains (ETH-Gaze by 0.12° and Gaze360 by 0.16°) and the unseen domains (MPIIFaceGaze by 0.60° and EyeDiap by 0.49°) compared to the baseline (ETH-Gaze+Gaze360), ultimately surpassing the best cross-domain generalization method GCF [34] (Gaze360) by a large improvement (*e.g.*, 7.26% in EyeDiap).

4.4 Domain Adaptation Results

Our previous experiments demonstrate the effectiveness of our method both in the source domain and in generalizing to unseen domains. To further validate the efficacy of our EIF framework, as done in previous domain generalization works [4, 34], we conduct additional domain adaptation experiments.

Similar with previous domain adaptation setting, we fine-tune the model with 100 images from the target domain. For our EIF, we use these data to constrain the evidence loss (Equation 14), both for all branches and their joint output after inter-fusion. For the baseline, we use these data to constrain the L1 loss. We trained each method for 100 batches, and to mitigate randomness resulting from the random sampling of the training set, we repeat the experiment 5 times and report the average results. As demonstrated in Table 2, our proposed cross-dataset gaze estimation training method significantly enhances domain adaptation performance. Notably, our EIF framework surpasses the cross-dataset baseline and achieves a reduction in angular error of 0.78° on MPIIFace and 0.29° on EyeDiap compared with the previous best single-dataset generalization method (*i.e.*, an average improvement of 12.62%).

Table 2: Comparison with SOTA methods in domain adaptation setting on 100 labeled samples. Results are shown in angle error (°).

Methods	Target Dataset		Avg
	MPIIFaceGaze	EyeDiap	
GCF (ETH-Gaze) [34]	4.76	5.43	5.10
GCF (Gaze360) [34]	5.34	5.66	5.50
PCFGaze (ETH-Gaze) [4]	4.74	5.88	5.31
PCFGaze (Gaze360) [4]	5.41	6.39	5.90
Baseline (ETH-Gaze+Gaze360)	3.96	5.26	4.61
EIF (ETH-Gaze+Gaze360)	3.98	5.14	4.56

Table 3: Ablation study of the single-dataset training on the ETH-Gaze Dataset.

L1 Regression	Evidential Regression	Intra-Evidential Fusion	Angle Error(°)
✓			5.02
	✓		5.07
	✓	✓	4.88

4.5 Ablation Study

Since our model consists of two stages, each serving a clear purpose: the first stage single-dataset training involves training a well-performing evidence learning regression branch for each dataset, while the second stage cross-dataset joint training entails fusing these branches based on evidence learning to achieve a model with superior generalization capability. Hence, for clarity, we conduct ablation experiments in two parts accordingly.

Single-dataset training: To train a well-performing single-dataset evidence learning regression branch, we primarily include two components: firstly, introducing evidential regression learning, and secondly, incorporating multiple local regressors corresponding to specific data subspaces and utilizing intra-evidential fusion to aggregate them. As shown in Table 3, we conduct ablation studies to evaluate the effectiveness of each components mentioned above: 1) Evidence regression: To estimate uncertainty, evidential regression introduces more complex distributions to model the regression, resulting in a slight error increase of 0.05°. However, this provides the foundation for our inter-intra evidence fusion; 2) Intra-evidential fusion: Compared to using only evidential regression in gaze estimation, the approach with the intra-evidential fusion strategy significantly reduces the angle error by 0.19°, surpassing the baseline method without evidence regression by 0.14°.

Cross-dataset joint training: To jointly train multiple single-dataset branches, we first adopt the inter-evidential fusion module to aggregate predictions from multiple branches. Additionally, we further designed a cross-dataset branch to integrate features from each branch. As shown in Table 4, we conduct ablation studies to evaluate the effectiveness of each module mentioned above. All the single-dataset branches used in this experiment are based on the intra-evidential fusion approach. The experimental result shows that inter-evidential fusion approach exhibits a significant reduction in errors compared to directly averaging prediction of each

Table 4: Ablation study for cross-dataset joint training. This study showcases the average angle errors (°) of the models trained on multiple source domains (ETH-Gaze+Gaze360) across the source domain test sets (ETH-Gaze and Gaze360) and the unseen domains (MPIIFaceGaze and EyeDiap).

Average Fusion	Inter-Evidential Fusion	Cross-Dataset Branch	Source	Unseen
✓			14.09	7.02
	✓		8.25	6.92
	✓	✓	8.14	6.66

Table 5: Parameter analysis in single-dataset training on ETH-Gaze dataset.

Parameter	Value	Angle Error (°)
G	4	4.92
	8	4.88
	16	4.93

branch after stage 1 (Average Fusion), with reductions of 5.84° and 0.1° in the source and unseen domains, respectively. These results match the preliminary experiment and clearly verify our intuition that aggregating predictions from multiple source domains with diverse distribution is beneficial for generalization even when employing a simple average fusion strategy. However, this simply fusion approach may compromise performance in the source domain. In contrast, our inter-fusion method not only significantly boosts performance in the source domain but also further amplifies it in the target domain. Moreover, our cross-dataset branch further enhances the performance of the inter-evidential fusion, with reductions of 0.11° and 0.26° in the source and unseen domains, respectively. This result highly suggests that our designed cross-dataset branch aggregates features from each source domain branch and thus can better fuse a wide range of distributions for generalization to unseen domains.

4.6 Parameter Sensitivity Analysis

In our experiments, we consider two critical hyperparameters: the number of local regressors G in single-dataset training and the MFF starting layer K in cross-dataset joint training. We separately conduct experiments to analyze the impact of these hyperparameters.

Effects of the number of local regressors in single-dataset training: As shown in Table 5, we can observe that within a certain range, adjusting the G has a relatively stable impact on the performance. Specifically, setting the number of local regressors to 8 achieves the best performance.

Effects of the layer K in cross-dataset joint training: As shown in Table 6, we can see that within a certain range, adjusting the K also has a relatively stable impact on the performance. In our experiment, setting K to 3 achieves the best performance.

4.7 Evidence Analysis

Evidential learning is crucial to our framework; we use it to achieve an inter-intra fusion, and the final evidential regression output

Table 6: Parameter analysis in cross-dataset training. Results are shown in angle error (°).

Param	Value	Dataset				
		Gaze360	ETH	MPII	EyeDiap	Avg
K	2	11.39	4.96	6.20	7.22	7.44
	3	11.33	4.95	6.41	6.90	7.40
	4	11.36	4.95	6.36	7.21	7.47

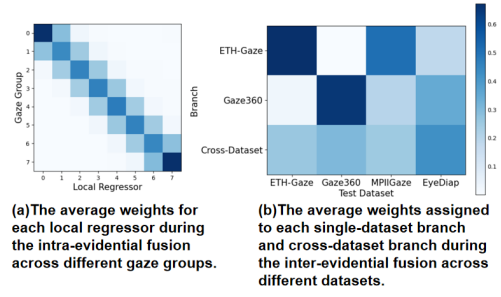
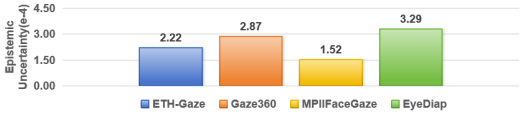
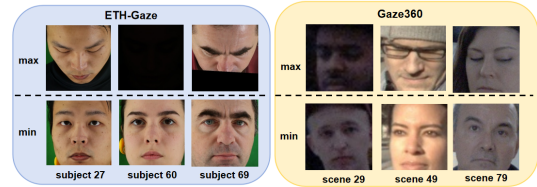
can also provide uncertainty estimations for robust predictions. Therefore, in this section, we offer a visual analysis of the fusion process and uncertainty predictions to validate the effectiveness of evidential learning in gaze estimation.

Inter-intra fusion visual analysis: Based on Equation 14, among the four output values of the evidential regression, δ represents the predicted gaze. Furthermore, according to Equation 11, during the evidential fusion process, normalized γ is employed as weights to aggregate δ accordingly. Hence, to further delve into our inter-intra evidential fusion module, we compute the mean normalized δ values spanning multiple local regressors or branches.

As depicted in Fig. 4(a), the visualization showcases the output on the yaw values of the test set corresponding to the single-dataset branch in ETH-Gaze. It is observable that the diagonal region possesses the highest values, indicating our intra-fusion module enables samples within each gaze group to find their corresponding local regressors effectively. Moreover, it is noted that the weights are not solely concentrated on a single diagonal but are diffused around the diagonal line. This distribution is attributed to our adoption of a density overlap strategy for gaze group segmentation (Equation 2), which allocates multiple experts to one sample in overlapping areas, thereby enhancing robustness. Conversely, due to the lack of overlap in the boundary gaze group areas (0 and 7), the weights are relatively more focused compared to other regions.

As shown in Fig. 4(b), the experiment is conducted on the complete EIF structure. It demonstrates that all source domain test sets have the highest weights on their respective single-dataset branches. On the other hand, in the unseen domains, the weights are distributed evenly across various branches. Notably, EyeDiap has the highest weight on the cross-dataset branch, while MPIIFaceGaze shows the highest weight on the ETH-Gaze branch. The possible reason is that the single-dataset branch learned on the ETH-Gaze dataset demonstrates a strong generalization capability on MPIIFaceGaze. Previous domain generalization methods in Table 1 have also shown that models trained on ETH-Gaze perform well on MPIIFaceGaze, which is consistent with this observation and verifies the effectiveness of our evidential learning fusion strategy.

Uncertainty Estimation Analysis: Our model can simultaneously provide epistemic uncertainty and aleatoric uncertainty. Epistemic uncertainty reflects the model’s uncertainty about the underlying structure of the data. It arises from the model’s lack of knowledge or exposure to certain regions of the input space during training. As shown in Fig. 5, the epistemic uncertainty of the unseen EyeDiap dataset is relatively large in our EIF structure’s final output, while that of the source domains and MPIIFaceGaze is

**Figure 4: Visualizing Weights During Inter-Intra Fusion.****Figure 5: The epistemic uncertainty of the dataset.****Figure 6: The aleatoric uncertainty of two source datasets**

smaller. The smaller uncertainty in MPIIFaceGaze may be due to its similarity to a subset of the source domain datasets.

The aleatoric uncertainty of the data involves the inherent uncertainty of the data itself, which cannot be eliminated even with a sufficiently large dataset. This uncertainty arises from factors such as low image quality, including reasons like image blur and occlusion of the eyes in our task. As depicted in Fig. 6, we showcase the aleatoric uncertainty output of our EIF in the source domain test sets, where ETH-Gaze is collected on a per-user basis, and Gaze360 is collected on a per-scene basis. Therefore, we respectively output the maximum and minimum values of the estimated aleatoric uncertainty for each subject or scene on ETH-Gaze and Gaze360. It can be observed that the aleatoric uncertainty output by our model effectively reflects the data quality in the source domain. More visualization results can be found in the appendix.

4.8 Computational Cost

Despite encompassing multiple branches, thanks to our two-stage learning strategy, our model can be trained swiftly to adapt to new scenarios. Once we have multiple trained single-dataset branches, our model requires only a minimal number of epochs in stage 2 to rapidly adjust to changes in the dataset, such as additions or deletions. Specifically, in our experiments, the training of stage 2 takes only 40 minutes on two NVIDIA TITAN XP GPU, whereas the baseline needs to start from scratch and mixing multiple datasets, which requires 5 hours for training.

5 CONCLUSION

Training with diverse source domain data can significantly improve the model's generalization ability in unseen domains. However, simple mixing may lead to adverse effects among datasets with inherent distribution shifts, thereby increasing their domain-specific errors. Our paper addresses these challenges by proposing a two-stage training approach. In the first stage, we utilize single dataset branches tailored to each source domain. Additionally, in stage 2, we conduct joint training of multiple single-dataset branches and introduce a cross-dataset branch to further aggregate the features extracted from the source domain branches. Considering the non-stationary nature of gaze behavior, we further divide individual source domain data into multiple subsets within each branch, each designed with a local regressor. We employ an evidential fusion strategy to integrate the predictions from various branches and local regressors. The experiments demonstrate the effectiveness of our method in both the source and unseen domains.

REFERENCES

- [1] Kenneth Alberto Funes Mora and Jean-Marc Odobez. 2014. Geometric generative gaze estimation (g3e) for remote rgb-d cameras. In *Proceedings of the IEEE Conference on Computer Vision and Pattern Recognition*. 1773–1780.
- [2] Alexander Amini, Wilko Schwarting, Ava Soleimany, and Daniela Rus. 2020. Deep evidential regression. *Advances in neural information processing systems* 33 (2020), 14927–14937.
- [3] Yiwei Bao, Yunfei Liu, Haofei Wang, and Feng Lu. 2022. Generalizing Gaze Estimation With Rotation Consistency. In *Proceedings of the IEEE/CVF Conference on Computer Vision and Pattern Recognition (CVPR)*. 4207–4216.
- [4] Yiwei Bao and Feng Lu. 2023. PCFGaze: Physics-Consistent Feature for Appearance-based Gaze Estimation. *arXiv preprint arXiv:2309.02165* (2023).
- [5] Xin Cai, Jiabei Zeng, Shiguang Shan, and Xilin Chen. 2023. Source-Free Adaptive Gaze Estimation by Uncertainty Reduction. In *Proceedings of the IEEE/CVF Conference on Computer Vision and Pattern Recognition (CVPR)*. 22035–22045.
- [6] Yanbei Chen, Manchen Wang, Abhay Mittal, Zhenlin Xu, Paolo Favaro, Joseph Tighe, and Davide Modolo. 2023. ScaleDet: A scalable multi-dataset object detector. In *Proceedings of the IEEE/CVF Conference on Computer Vision and Pattern Recognition*. 7288–7297.
- [7] Yihua Cheng, Yiwei Bao, and Feng Lu. 2022. Puregaze: Purifying gaze feature for generalizable gaze estimation. In *Proceedings of the AAAI Conference on Artificial Intelligence*, Vol. 36. 436–443.
- [8] Yihua Cheng and Feng Lu. 2023. Dvgaze: Dual-view gaze estimation. In *Proceedings of the IEEE/CVF International Conference on Computer Vision*. 20632–20641.
- [9] Yihua Cheng, Haofei Wang, Yiwei Bao, and Feng Lu. 2021. Appearance-based gaze estimation with deep learning: A review and benchmark. *arXiv preprint arXiv:2104.12668* (2021).
- [10] Yimian Dai, Fabian Gieseke, Stefan Oehmcke, Yiquan Wu, and Kobus Barnard. 2021. Attentional Feature Fusion. In *IEEE Winter Conference on Applications of Computer Vision, WACV 2021*.
- [11] Philippe Ambrozio Dias, Damiano Malafronte, Henry Medeiros, and Francesca Odone. 2020. Gaze estimation for assisted living environments. In *Proceedings of the IEEE/CVF Winter Conference on Applications of Computer Vision*. 290–299.
- [12] Hao-Shu Fang, Jiefeng Li, Hongyang Tang, Chao Xu, Haoyi Zhu, Yuliang Xiu, Yong-Lu Li, and Cewu Lu. 2022. Alphapose: Whole-body regional multi-person pose estimation and tracking in real-time. *IEEE Transactions on Pattern Analysis and Machine Intelligence* (2022).
- [13] Kenneth Alberto Funes Mora, Florent Monay, and Jean-Marc Odobez. 2014. Eye-diap: A database for the development and evaluation of gaze estimation algorithms from rgb and rgb-d cameras. In *Proceedings of the symposium on eye tracking research and applications*. 255–258.
- [14] Shreya Ghosh, Abhinav Dhall, Munawar Hayat, Jarrod Knibbe, and Qiang Ji. 2023. Automatic gaze analysis: A survey of deep learning based approaches. *IEEE Transactions on Pattern Analysis and Machine Intelligence* 46, 1 (2023), 61–84.
- [15] Thomas Gilles, Stefano Sabatini, Dzmirty Tsishkou, Bogdan Stanculescu, and Fabien Moutarde. 2022. Uncertainty estimation for Cross-dataset performance in Trajectory prediction. *arXiv preprint arXiv:2205.07310* (2022).
- [16] Zidong Guo, Zejian Yuan, Chong Zhang, Wanchao Chi, Yonggen Ling, and Shenghao Zhang. 2020. Domain adaptation gaze estimation by embedding with prediction consistency. In *Proceedings of the Asian Conference on Computer Vision*.
- [17] Dan Witzner Hansen and Qiang Ji. 2009. In the eye of the beholder: A survey of models for eyes and gaze. *IEEE transactions on pattern analysis and machine intelligence* 32, 3 (2009), 478–500.
- [18] Ming Jiang and Qi Zhao. 2017. Learning visual attention to identify people with autism spectrum disorder. In *Proceedings of the IEEE international conference on computer vision*. 3267–3276.
- [19] Petr Kellnhofer, Adria Recasens, Simon Stent, Wojciech Matusik, and Antonio Torralba. 2019. Gaze360: Physically unconstrained gaze estimation in the wild. In *Proceedings of the IEEE/CVF international conference on computer vision*. 6912–6921.
- [20] Joohwan Kim, Michael Stengel, Alexander Majercik, Shalini De Mello, David Dunn, Samuli Laine, Morgan McGuire, and David Luebke. 2019. Nvgaze: An anatomically-informed dataset for low-latency, near-eye gaze estimation. In *Proceedings of the 2019 CHI conference on human factors in computing systems*. 1–12.
- [21] Wanhua Li, Jiwen Lu, Jianjiang Feng, Chunjing Xu, Jie Zhou, and Qi Tian. 2019. Bridgenet: A continuity-aware probabilistic network for age estimation. In *Proceedings of the IEEE/CVF conference on computer vision and pattern recognition*. 1145–1154.
- [22] Ruicong Liu, Yunfei Liu, Haofei Wang, and Feng Lu. 2024. PnP-GA+: Plug-and-Play Domain Adaptation for Gaze Estimation using Model Variants. *IEEE Transactions on Pattern Analysis and Machine Intelligence* (2024).
- [23] Wenbo Liu, Ming Li, and Li Yi. 2016. Identifying children with autism spectrum disorder based on their face processing abnormality: A machine learning framework. *Autism Research* 9, 8 (2016), 888–898.
- [24] Yunfei Liu, Ruicong Liu, Haofei Wang, and Feng Lu. 2021. Generalizing gaze estimation with outlier-guided collaborative adaptation. In *Proceedings of the IEEE/CVF International Conference on Computer Vision*. 3835–3844.
- [25] Jieming Lou, Weide Liu, Zhuo Chen, Fayao Liu, and Jun Cheng. 2023. Elnet: Evidential local-global fusion for stereo matching. In *Proceedings of the IEEE/CVF International Conference on Computer Vision*. 17784–17793.
- [26] Huan Ma, Zongbo Han, Changqing Zhang, Huazhu Fu, Joey Tianyi Zhou, and Qinghua Hu. 2021. Trustworthy multimodal regression with mixture of normal-inverse gamma distributions. *Advances in Neural Information Processing Systems* 34 (2021), 6881–6893.
- [27] Päivi Majaranta and Andreas Bulling. 2014. Eye tracking and eye-based human-computer interaction. In *Advances in physiological computing*. Springer, 39–65.
- [28] Anjul Patney, Joohwan Kim, Marco Salvi, Anton Kaplanyan, Chris Wyman, Nir Benty, Aaron Lefohn, and David Luebke. 2016. Perceptually-based foveated virtual reality. In *ACM SIGGRAPH 2016 emerging technologies*. 1–2.
- [29] Rima-Maria Rahal and Susann Fiedler. 2019. Understanding cognitive and affective mechanisms in social psychology through eye-tracking. *Journal of Experimental Social Psychology* 85 (2019), 103842.
- [30] Bowen Shi, Xiaopeng Zhang, Haochang Xu, Wenrui Dai, Junni Zou, Hongkai Xiong, and Qi Tian. 2021. Multi-dataset pretraining: A unified model for semantic segmentation. *arXiv preprint arXiv:2106.04121* (2021).
- [31] Roberto Valenti, Nicu Sebe, and Theo Gevers. 2011. Combining head pose and eye location information for gaze estimation. *IEEE Transactions on Image Processing* 21, 2 (2011), 802–815.
- [32] Li Wang, Dong Li, Han Liu, Jinzhang Peng, Lu Tian, and Yi Shan. 2022. Cross-dataset collaborative learning for semantic segmentation in autonomous driving. In *Proceedings of the AAAI Conference on Artificial Intelligence*, Vol. 36. 2487–2494.
- [33] Yaoming Wang, Yangzhou Jiang, Jin Li, Bingbing Ni, Wenrui Dai, Chenglin Li, Hongkai Xiong, and Teng Li. 2022. Contrastive regression for domain adaptation on gaze estimation. In *Proceedings of the IEEE/CVF Conference on Computer Vision and Pattern Recognition*. 19376–19385.
- [34] Mingjie Xu, Haofei Wang, and Feng Lu. 2023. Learning a generalized gaze estimator from gaze-consistent feature. In *Proceedings of the AAAI conference on artificial intelligence*, Vol. 37. 3027–3035.
- [35] Yongqiang Yao, Yan Wang, Yu Guo, Jiaojiao Lin, Hongwei Qin, and Junjie Yan. 2020. Cross-dataset training for class increasing object detection. *arXiv preprint arXiv:2001.04621* (2020).
- [36] Xumin Yu, Yongming Rao, Wenliang Zhao, Jiwen Lu, and Jie Zhou. 2021. Group-aware contrastive regression for action quality assessment. In *Proceedings of the IEEE/CVF international conference on computer vision*. 7919–7928.
- [37] Jiabei Zeng, Shiguang Shan, and Xilin Chen. 2018. Facial expression recognition with inconsistently annotated datasets. In *Proceedings of the European conference on computer vision (ECCV)*. 222–237.
- [38] Xucong Zhang, Seonwook Park, Thabo Beeler, Derek Bradley, Siyu Tang, and Otmir Hilliges. 2020. Eth-xgaze: A large scale dataset for gaze estimation under extreme head pose and gaze variation. In *Computer Vision—ECCV 2020: 16th European Conference, Glasgow, UK, August 23–28, 2020, Proceedings, Part V 16*. Springer, 365–381.
- [39] Xucong Zhang, Yusuke Sugano, Mario Fritz, and Andreas Bulling. 2017. Mpiigaze: Real-world dataset and deep appearance-based gaze estimation. *IEEE transactions on pattern analysis and machine intelligence* 41, 1 (2017), 162–175.